FEM Analysis of Micromachined Flow Sensor with Wheatstone Bridge Read-out

A. Talić[*,1], S. Ćerimović[1], F. Kohl[1], R. Beigelbeck[1], F. Keplinger[2] and J. Schalko[1,2]
[1]Research Unit for Integrated Sensor Systems, Austrian Academy of Sciences, Wr. Neustadt, Austria
[2]Institute of Sensor and Actuator Systems, Vienna University of Technology, Vienna, Austria
*Corresponding author: Research Unit for Integrated Sensor Systems, Viktor Kaplan Str. 2,
A-2700 Wiener Neustadt, Austria, almir.talic@oeaw.ac.at

Abstract: In this work, we present simulations of a novel micromachined calorimetric flow sensor using COMSOL software. It is based on four germanium thermistors embedded in a thin silicon nitride membrane. These thermistors serve as heat sources and as temperature sensors simultaneously. In operational mode, the heated membrane is cooled by any passing flow and the local cooling rate depends on the flow velocity. The thermistors are connected to form a Wheatstone bridge, which is supplied by a constant current. As output quantities, we analyze the voltage across the bridge U_B as well as the voltage at the bridge supply terminals U_{SUP}. The simulation results demonstrate the feasibility of the new concept and suggest that high flow sensitivities and fast response times in combination with extremely low power consumption can be accomplished.

Keywords: FEM analysis, calorimetric flow sensors, Wheatstone bridge configuration, heat transfer module

1. Introduction

Many modern technical products like cars, process monitors, mass production equipment, or domestic appliances are equipped with flow sensors to provide sufficient information for controlled operation. Micromachining is the preferred production method for such sensors in order to achieve high sensitivity, quick response, improved durability as well as low power consumption. Commonly used micromachined calorimetric flow sensors feature heat source(s) and spatially separated temperature sensors, which both are embedded in a thin membrane [1]. Two temperature sensors measure the local temperature at a position upstream and downstream of the heat source. Without fluid flow, the temperature field generated by the heat source is symmetrical. Any tangential flow next to the sensor surface disturbs this thermal symmetry. Upstream of the heater, the membrane temperature decreases with increasing distance from the heater, indicating that the convective cooling is very efficient in this region. Downstream of the heater, the fluid temperature may become even higher than the surface temperature resulting in a local heating of the sensor membrane. The upstream/downstream temperature difference is converted into an output voltage, which can be used as a measure for the fluid velocity or mass flow. The flow range and sensitivity is strongly influenced by the distance between heater and temperature sensors [3, 4].
In this paper, we perform FEM simulations of a micromachined flow sensor exhibiting a novel transduction approach. Contrary to the standard layout with a thin-film heating resistor [2], we utilize four germanium thermistors embedded in the silicon membrane. They act as distributed heat sources and as temperature sensors at the same time. The thermistors are connected to form a Wheatstone bridge that can be read out, e.g., with a high-impedance galvanometer (see Figure 1).

2. Flow Sensor design

Figure 1 shows the cross section of micromachined calorimetric flow sensors. The sensor membrane consists of the SiO_2 and Si_3N_4 wafer coating, and the passivation layer SiN_x, featuring 150 nm, 200 nm, and 1250 nm thickness, respectively. For the sake of simplicity, our simulation combines the first two layers to one bottom layer using averaged thermal properties. The four thermistors are manufactured on the bottom layer and placed symmetrically to membrane midpoint at the distances of 75 μm and 150 μm, respectively. Each of them consists of a 220 nm thick germanium film, which is contacted by four metal strips exhibiting a Ti-Au-Cr sandwich (total thickness 180 nm). The sensor membrane features an overall thickness of about 1.6 μm and is supported by a micromachined silicon frame (350 μm thick). The sensor device is mounted flush with the wall of a flow channel (height 1 mm). The dimensions of all model elements with the material parameters are listed in Table 1.

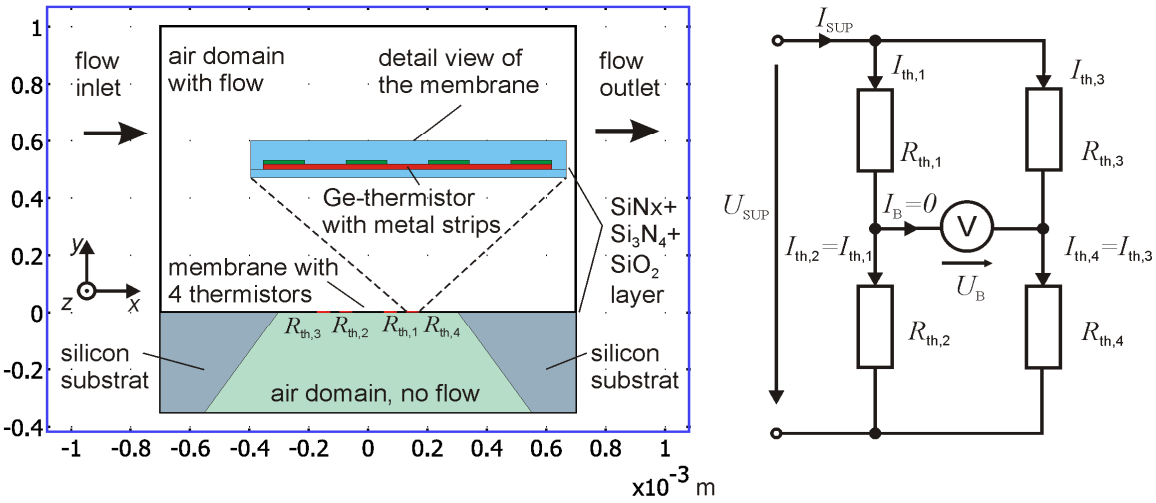

Figure 1. Simplified 2D-model and Wheatstone bridge comprising four membrane thermistors.

3. Modelling and Simulation

We simulated the static and transient behaviour of the airflow sensor. The FEM analysis was based on the schematic cross section indicated in Figure 1. A two dimensional (2D) model seems reasonable since all thin-film components on the membrane exhibit a large extension perpendicular to the flow direction. Figure 1 depicts the arrangement of the membrane components used for simulations. Based on the heat transfer equation, the employed heat transport model includes conduction and convection, whereas radiative heat transfer was neglected:

$$\rho C_p \frac{\partial T}{\partial t} + \nabla \cdot (-k \nabla T + \rho C_p T \mathbf{u}) = Q, \qquad (1)$$

where T, ρ, k, and C_p denotes the temperature, the density, the thermal conductivity, and the heat capacity of the medium, respectively. Q denotes the density of supplied heat source and **u** represents the local velocity. Furthermore, the temperature dependencies of viscosity, density, heat capacity, and thermal conductivity of the fluid have been neglected and consequentially the effects of natural convection were not treaded.

The sensor model comprises two air domains. Convective heat transfer is only considered in the upper one. The fluid velocity in x-direction is imposed as parabolic function [5] with respect to the y-coordinate implying the non-slip boundary condition at the top and bottom flow channel walls

$$u_x = v_{in} \cdot 1.5 \cdot \left(1 - \frac{y - \frac{d_y}{2}}{\frac{d_y}{2}} \right)^2 \cdot f_{corr}. \qquad (2)$$

v_{in} is the average flow velocity at flow inlet and d_y is the channel height. f_{corr} denotes a correction factor, which takes into account the effect of the finite channel width d_z on the flow profile. The 2D simulation model, however, assumes infinite channel width with respect to the z-direction. The actual flow profile has the form of a paraboloid

$$u_x = v_{in} \cdot 1.5 \cdot \left(1 - \frac{y - \frac{d_y}{2}}{\frac{d_y}{2}} \right)^2 \cdot 1.5 \cdot \left(1 - \frac{z - \frac{d_z}{2}}{\frac{d_z}{2}} \right)^2, \qquad (3)$$

where d_y and d_z referes the channel height and width, respectively. Averaging (3) over the extension of the thermistor in z-direction (600 µm) yields f_{corr}= 1.375. The fluid velocity in y-direction is assumed to be zero (u_y=0).

The boundary condition at the outlet of the flow compartment is implemented as convective flux, the remaining parts of the model circumference were kept at the ambient temperature (T_{amb} = 21°C). This is also the initial temperature value for all domains. The electrical thermistor resistance is modelled as

$$R_{th,i}(\vartheta) = R_{th,0} \cdot e^{\alpha \vartheta_i}, \quad i = 1...4, \qquad (4)$$

where α = –0.0179 /°C is the temperature coefficient of resistivity and $R_{th,0}$ = 200 kΩ the thermistor resistance at ϑ_i = 0°C. The thermistor temperatures ϑ_i were calculated through a subdomain integration of the variable T over each thermistor area. Figure 2 shows the simulated temperature field distribution for v_{in}= 10 m/s. The flow direction is indicated by red arrows. The length of these arrows scales with the local magnitude of the flow velocity.

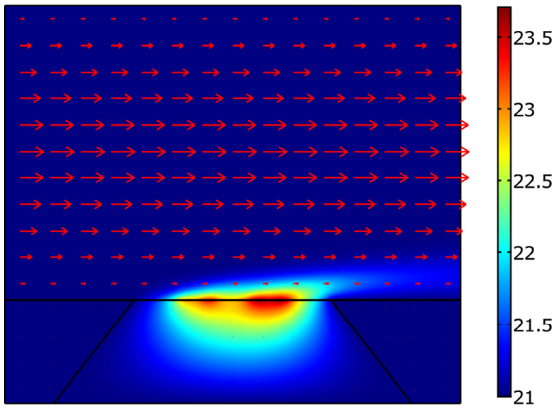

Figure 2. Simulated temperature distribution at the symmetry plane of the sensor for an average flow velocity of 10 m/s (parabolic flow profile in the channel). Boundary temperatures amount to $T_{amb} = 21°C$. The flow direction in the channel is indicated by red arrows.

The density of the dissipated power in the thermistor equals

$$Q_i = \frac{I_{th,i}^2 R_{th,i}(\vartheta_i)}{V}, \quad i = 1...4, \tag{5}$$

where V specifies the thermistor volume and $I_{th,i}$ is the thermistor current. It depends indirectly on ϑ_i due to the thermistor effect. The thermistors currents are expressible by

$$I_{th,1} = I_{th,2} = I_{SUP} \frac{R_{th,3} + R_{th,4}}{R_{th,1} + R_{th,2} + R_{th,3} + R_{th,4}}, \tag{6}$$

$$I_{th,3} = I_{th,4} = I_{SUP} \frac{R_{th,1} + R_{th,2}}{R_{th,1} + R_{th,2} + R_{th,3} + R_{th,4}}, \tag{7}$$

where I_{SUP} denotes the bridge supply current. All thermistor temperatures are influenced by convective heat transfer on the one hand and the power dissipation Q_i on the other hand, which in turn depends on the temperature (Eqs. (4) and (5)). Starting from the initial temperature, the values $R_{th,I}$, $I_{th,I}$, and hence Q_i are computed. The first value of Q_i is imposed and the thermistor temperatures are calculated anew. In next computational steps, Q_i is updated until a steady-state is reached.

4. Results and Discussion

The presented electrocalorimetric flow sensor consists of four temperature sensors connected to form a Wheatstone bridge. This configuration benefits from two features: First, it provides all four thermistors with the necessary current. Second, it utilizes the temperature variation of each of them to generate a bias-free output signal. In order to avoid the destruction of the thermistors due to their NTC-characteristic, we supplied the bridge with a constant electric current $I_{SUP} = 50\ \mu A$ ensuring that the thermistor voltages do not exceed the rated value of 5 V. Moreover, the low current limits the power consumption (~ 0.3 mW).

The voltage across the bridge U_B depends on the thermistor resistance values and hence on the flow velocity

$$U_B = I_{SUP} \frac{R_{th2}R_{th3} - R_{th1}R_{th4}}{R_{th1} + R_{th2} + R_{th3} + R_{th4}}. \tag{8}$$

The thermistors embedded in the silicon membrane act as heat sources and as temperature sensors at the same time. For zero flow, the temperature profile inside the membrane is symmetrical. Therefore, the outer thermistors R_{th3} and R_{th4} exhibit the same temperature. The inner thermistors R_{th1} and R_{th2} behave in the same way. Any flow passing by the membrane's surface deforms the temperature profile inside the membrane, which is converted into flow magnitude by means of the thermistors. With increasing flow, the thermistors next to flow inlet ($R_{th,2}$ and $R_{th,3}$) are cooled down more efficient than the thermistors near the flow outlet ($R_{th,1}$ and $R_{th,4}$). Hence, by connecting the thermistors as shown in Figure 1, one achieves the best possible sensitivity. Figure 3 shows the dependence of thermistor temperatures ϑ_i on the average flow velocity.

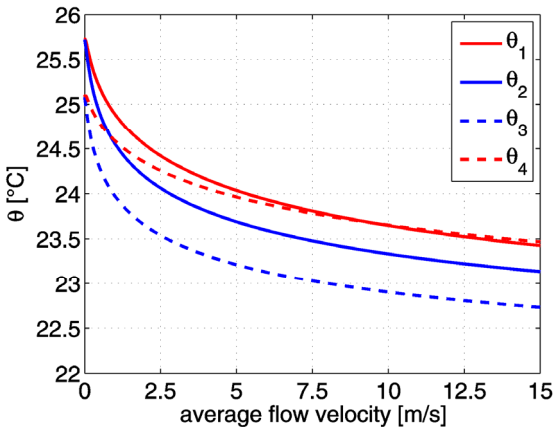

Figure 3. Thermistor temperatures ϑ_i over the average flow velocity.

Beside U_B, the voltage at the bridge supply terminals U_{SUP} also depends on the flow velocity and can be used as an additional output quantity

$$U_{SUP} = I_{SUP} \frac{(R_{th1} + R_{th2})(R_{th3} + R_{th4})}{R_{th1} + R_{th2} + R_{th3} + R_{th4}}. \tag{9}$$

Based on this sensor concept, we performed steady flow and flow step (transient) simulations to analyse the device behaviour.

4.1 Steady flow simulations

The steady flow simulations were conducted up to an average flow velocity of v_{in}= 15 m/s. For higher velocities the flow in the channel could become turbulent. As an output quantity, we analyzed both, the voltage across the bridge U_B and the voltage at the bridge supply terminals U_{SUP} (see Figure 4).

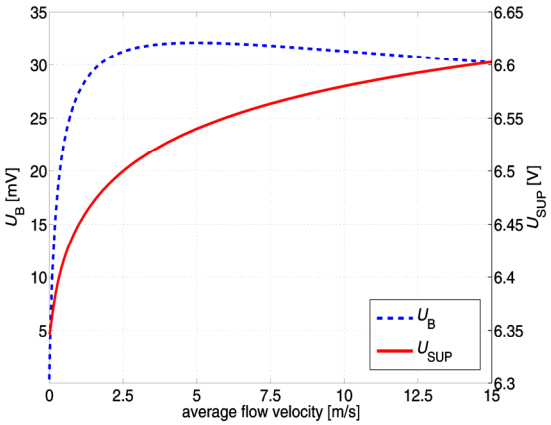

Figure 4. Output characteristics of the flow sensor using the voltage across the bridge U_B and the voltage at the bridge supply terminals U_{SUP} as an output quantity.

Evaluating the voltage across the bridge, an excellent sensitivity for flow velocities below 2 m/s is found. However, for higher velocities, the output characteristic becomes ambiguous. Therefore the use of U_{SUP} as an output quantity is desired resulting in a wider measurement range but poorer sensitivity for lower flow velocities.

4.2 Flow step simulations

Simulations of the transient behaviour in response to a flow step were also conducted. For this purpose, the stationary simulation results for v_{in}= 0 m/s (no flow) were used as initial state. The simulated response of U_B and U_{SUP} to flow steps is shown in Figure 5 and 6. The rise time depends for both functions on the height of the flow step. In case of U_B the simulated rise time is of the order of only few milliseconds. The flow step response exhibits a small to intermediate overshoot depending on the height of the flow step. In case of U_{SUP}, the flow step response features the long rise time of up to 22 ms (for v_{in}= 5 m/s) but without any overshoot.

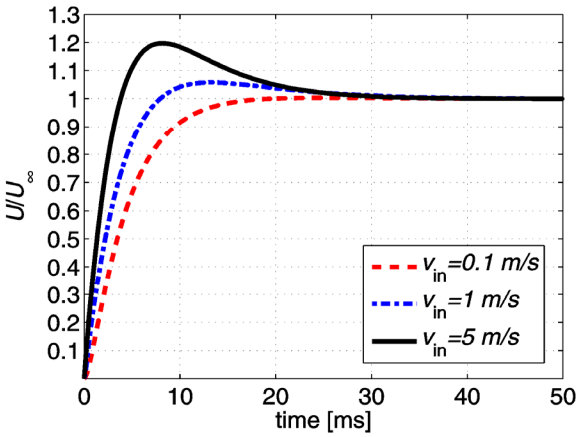

Figure 5. Relative flow step response of the bridge voltage U_B for different heights of the flow step (U_∞ is the final value).

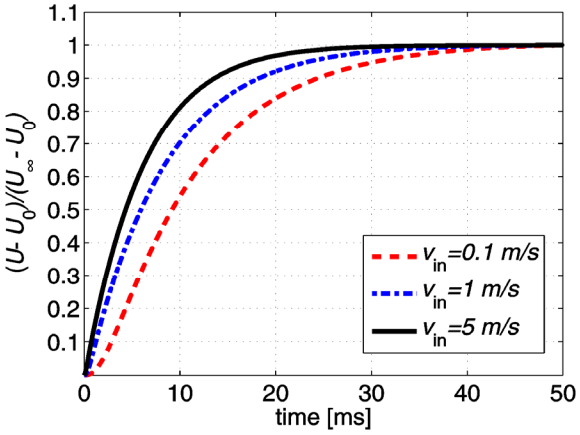

Figure 6. Relative flow step response of the bridge supply terminals voltage U_{SUP} for different heights of the flow step (U_0 is the initial value, U_∞ is the final value).

5. Conclusions

We performed FEM simulations of a micromachined flow sensor featuring four germanium thermistors embedded in a silicon nitride membrane. The thermistors were connected to form a Wheatstone bridge. As an output quantity, we analyzed both, the voltage across the bridge U_B and the voltage at the bridge supply terminals U_{SUP} assuming a constant supply current. Evaluating the bridge voltage for steady flow, an excellent sensitivity for flow velocities below 2 m/s was achieved. For higher velocities, the output characteristic becomes ambiguous. The rise time of the flow step response is in the order of only few milliseconds. On the other hand U_{SUP} offers a wider measurement range but poorer sensitivity at lower velocities. The rise time amounts up to 20 ms.

6. Outlook

The 2D FEM analysis is a convenient tool to predict the behaviour of our sensor design. In next future, we focus on design optimization topics and manufacturing of the novel flow sensor. A detailed comparison of FEM simulation, analytical model, and measurement will be subject of further investigations.

7. References

[1] N. Sabaté, J. Santander, L. Fonseca, I. Gràcia, C. Cané, Multi-range silicon micromachined flow sensor, Sensors and Actuators A 110 (2004) 282–288.

[2] F. Kohl, R. Fasching, F. Keplinger, R. Chabicovsky, A. Jachimowicz, G. Urban, Development of miniaturized semiconductor flow sensors, Measurement 33 (2003) 109–119.

[3] L. Qui, S. Hein, E. Obermeier, A. Schubert, Micro gas-flow sensor with integrated heat sink and flow quide, Sensors Actuators A 54 (1996) 547-551.

[4] U. Dillner, E. Kessler, S. Poser, V. Baier, J. Müller, Low power consumption thermal gas-flow sensor based on thermopiles of highly effective thermoelectric materials, Sensor Actuators A 60 (1997) 1-4.

[5] H. Schlichting and K. Gersten, Grenzschicht-Theorie. Springer Press (Berlin, Heidelberg, New York) (1997) 110-111.

8. Acknowledgements

We gratefully acknowledge partial financial support by the Austrian Science Fund FWF (research grant L234-N07).

9. Appendix

Table 1. List of model elements with material parameters.

sensor chip	silicon substrat	height	350 µm
		bottom width	150 µm
		top width	397 µm
		ρ	2329 kg/m³
		k	130 W/mK
		C_p	700 J/kgK
	Si_3N_4+ SiO_2 layer	thickness	350 nm
		width	1.4 mm
		ρ	2765.7 kg/m³
		k (anisotropic)	| 1.91 0 | | 0 1.8 | W/mK
		C_p	710.2 J/kgK
	SiN_x layer	thickness	1250 nm
		width	1.4 mm
		ρ	2800 kg/m³
		k	0.8 W/mK
		C_p	620 J/kgK
	thermistor	thickness	220 nm
		width	35 µm
		ρ	5323 kg/m³
		k	0.5 W/mK
		C_p	310 J/kgK
	metal strips	thickness	180 nm
		width	5 µm
		spacing	5 µm
		ρ	13165.5 kg/m³
		k (anisotropic)	| 107.8 0 | | 0 55.4 | W/mK
		C_p	158.8 J/kgK
air domain	with flow (flow channel)	height	1 mm
		width	1.4 mm
	no flow	height	350 µm
		bottom width	1100 µm
		top width	606 µm
	both	ρ	1.032 kg/m³
		k	0.026 W/mK
		C_p	1099 J/kgK